Available online at www.sciencedirect.com

SCIENCE DIRECT®

Journal of Computational Physics 207 (2005) 405–426

JOURNAL OF COMPUTATIONAL PHYSICS

www.elsevier.com/locate/jcp

The kinematic Laplacian equation method

F.L. Ponta [1]

Department of Theoretical and Applied Mechanics, University of Illinois at Urbana-Champaign, Urbana, IL 61801, USA

Received 18 May 2004; received in revised form 30 November 2004; accepted 6 January 2005
Available online 25 February 2005

Abstract

A novel procedure for the Navier–Stokes equations in the vorticity–velocity formulation is presented. The time evolution of the vorticity is solved as an ODE problem on each node of the spatial discretization, using at each step of the time discretization the spatial solution for the velocity field provided by a new PDE expression called the kinematic Laplacian equation (KLE). This complete decoupling of the two variables in a vorticity-in-time/velocity-in-space split algorithm reduces the number of unknowns to solve in the time-integration process and also favors the use of advanced ODE algorithms enhancing the efficiency and robustness of time integration. The issue of the imposition of vorticity boundary conditions is addressed, as well as the details of the implementation of the KLE by isoparametric finite element discretization. We shall see some validation results of the KLE method applied to the classical case of a circular cylinder in impulsive-started pure-translational steady motion at several Reynolds numbers in the range $5 < Re < 180$, comparing them with experimental measurements and flow visualization plates; and finally, a recent result from a study on periodic vortex-array structures produced in the wake of forced-oscillating cylinders.
© 2005 Elsevier Inc. All rights reserved.

Keywords: Vorticity–velocity formulation; Navier–Stokes equations; Time-space split algorithm; Finite element method

1. Introduction

During the last three decades several studies appeared concerning the representation of the Navier–Stokes equations in terms of nonprimitive variables (namely the vorticity and the velocity potentials) instead of the classical formulation in terms of the primitive variables velocity and pressure. This family of approaches generally known as vorticity-stream function (ω, ψ) methods have proven to be quite effective. Especially for the case of incompressible two-dimensional flows, they offer the advantages of

E-mail address: ponta@uiuc.edu.

[1] Also at: College of Engineering, University of Buenos Aires.

0021-9991/$ - see front matter © 2005 Elsevier Inc. All rights reserved.
doi:10.1016/j.jcp.2005.01.014

reducing the number of unknowns and of eliminating the incompressibility condition. They have also been applied successfully to three-dimensional cases in spite of certain difficulties associated with the specification of the boundary conditions for the velocity potentials in particular in multiply-connected domains. A comprehensive study of this methods can be found in Quartapelle [1] where the crucial issue of the boundary conditions is analyzed in detail. For more recent references the reader may consult [2,3].

1.1. Hybrid vorticity–velocity formulation

More recently, together with those works on the vorticity-stream function formulation and as a natural extension of them, a comparatively smaller number of studies were presented using a hybrid formulation in terms of the primitive and nonprimitive variables velocity and vorticity. As several authors pointed out, the vorticity–velocity ($\boldsymbol{\omega}$, $\boldsymbol{v}$) methods (as they are generally known) present some advantages compared with the classical formulation on primitive variables or with the vorticity-stream function methods [1,4,5], namely:

- The pair of variables involved is particularly suited for a dynamic description of incompressible viscous flows. The vorticity is governed by a well understood dynamical equation while the velocity, which embodies the kinematical aspect of the problem, can be related to the vorticity by a simple elliptic equation. In vortex-dominated flows the vorticity advection is a fundamental process determining the dynamics of the flow, hence the vorticity–velocity description is closer to physical reality.
- The variety of boundary conditions that can be chosen for the velocity potentials due to the nonuniqueness of the velocity representation is avoided since the velocity is supplemented by unique boundary conditions.
- In some specific situations like that of external flows, boundary conditions at infinity are easier to implement for the vorticity than for the pressure.
- The noninertial effects only enter the solution procedure of the ($\boldsymbol{\omega}$, $\boldsymbol{v}$) formulation via the proper implementation of the initial and boundary conditions. Hence, the general applicability of an algorithm based on the ($\boldsymbol{\omega}$, $\boldsymbol{v}$) formulation is enhanced because it is independent of whether or not the frame of reference is inertial.
- The ($\boldsymbol{\omega}$, $\boldsymbol{v}$) formulation can match the equations of the boundary layer theory more easily than the primitive variable formulation.
- The study of the inviscid limit of the Navier–Stokes equations to the Euler equations for incompressible flows can be made easier by the elimination of the pressure variable.
- The most natural relation between vortex/particle methods and the Navier–Stokes equations is the ($\boldsymbol{\omega}$, $\boldsymbol{v}$) formulation of the latter and a better understanding of vortex methods in the presence of no-slip boundaries could be eventually achieved.

The first uses of the ($\boldsymbol{\omega}$, $\boldsymbol{v}$) formulation of the incompressible Navier–Stokes equations were reported by Fasel [6] who analyzed the stability of boundary layers in two dimensions and by Dennis, Ingham and Cook [7] who derived a numerical method for computing steady-state three-dimensional flows. Both approach were based on finite difference techniques. Since then several investigations have been conducted on incompressible hybrid variable models using variations of the finite difference approach (e.g., see [8–10], among others). A vorticity–velocity finite element solution of the three-dimensional compressible Navier–Stokes equations have been presented by Guevremont et al. [11] who investigated the steady state flow in a cubic cavity for several Mach numbers. More recently Clerxc [4], then Davies and Carpenter [12], introduced pseudospectral procedures for the ($\boldsymbol{\omega}$, $\boldsymbol{v}$) formulation. Lo and Young [13] presented an arbitrary Lagrangian–Eulerian ($\boldsymbol{\omega}$, $\boldsymbol{v}$) method for two-dimensional free surface flow, using finite difference discretization for the free surface and finite element discretization for the interior of the domain.

A disadvantage of the vorticity–velocity formulation, compared with the formulation in primitive variables is that in the most general three-dimensional case the $(\boldsymbol{\omega}, \boldsymbol{v})$ formulation requires a total of six equations to be solved instead of the usual four of the primitive-variable approach [4]. The objective of the present study is to introduce a new method based on the $(\boldsymbol{\omega}, \boldsymbol{v})$ formulation which aims to tackle this six-unknown question and to improve some other aspects of the numerical implementation of the $(\boldsymbol{\omega}, \boldsymbol{v})$ approach. This alternative method is characterized by a complete decoupling of the two variables in a vorticity-in-time/velocity-in-space split algorithm, thus reducing to three the number of unknowns to solve in the time integration process. As we shall see later on, this time-space splitting also favors the use of adaptive variable-stepsize/variable-order ODE algorithms which enhances the efficiency and robustness of the time integration process.

A comprehensive study of the theoretical basis of the vorticity–velocity formulation in two and three dimensions can be found in Chapter 4 of Quartapelle [1], including a series of theorems proving the equivalence between the $(\boldsymbol{\omega}, \boldsymbol{v})$ formulation of the incompressible Navier–Stokes equations and their classical formulation in primitive variables (velocity–pressure).

1.2. Vorticity boundary conditions

A common problem to all the methods based on nonprimitive or hybrid variables is the absence of boundary conditions for the vorticity in presence of no-slip boundary conditions for the velocity. In the case of the $(\boldsymbol{\omega}, \boldsymbol{\psi})$ formulation it also implies that the Poisson problem for the stream function with both Dirichlet and Neumann conditions is overdetermined. There are several different ways of overcoming this difficulty. Some earlier approaches like the *boundary vorticity formula* or the *vorticity creation* methods use different techniques to define the boundary values of vorticity in terms of the stream function (or the velocity) by means of some approximate formula applied locally at the no-slip boundary. They are roughly equivalent, however their implementation may differ remarkably depending on the type of discretization used (see [1,14–16]). Two other options to circumvent the problem of vorticity boundary conditions are either eliminating the vorticity variable from the formulation introducing a single biharmonic equation for the stream-function, or regarding the two second-order partial differential equations for $\boldsymbol{\omega}$ and $\boldsymbol{\psi}$ as constituting a system of two coupled equations, the coupling being engendered by the double specification on the boundary for one variable [1].

An alternative viewpoint have been introduced by Quartapelle and Valz-Gris [17,18]. They showed that in order to satisfy the no-slip boundary conditions for the velocity, the vorticity should be subject to an integral constraint. This integral condition enforces the orthogonality of the abstract projection of the vorticity field with respect to the linear space of the harmonic functions defined on the domain. This condition is a direct consequence of the boundary conditions on the velocity, and ensure satisfaction of essential conservation laws for the vorticity. An important aspect of the integral vorticity conditions is their nonlocal character: the vorticity distribution in the interior of the domain and on its boundary is affected at each time by the instantaneous values of the tangential and normal components of the velocity along the entire boundary. In other words, the distribution of the vorticity in the whole domain is constrained by the velocity boundary values. There are several ways for satisfying the vorticity integral conditions and performing the underlying orthogonal projection. However, this orthogonal-projection operation may be generally schematized as follows: First, a "wrong" vorticity field $\boldsymbol{\omega}^0$ is computed solving a time-discretized version of the vorticity transport equation assuming arbitrary values on the no-slip boundary (for instance, homogeneous conditions). Then, the sought solution $\boldsymbol{\omega}$ is obtained by enforcing the orthogonality of $\boldsymbol{\omega}^0$ with respect to the linear space of the harmonic functions. A detailed description of the mathematical basis and the different numerical implementations of the orthogonal-projection operation of the vorticity field for the $(\boldsymbol{\omega}, \boldsymbol{\psi})$ formulation can be found in [1].

2. The kinematic Laplacian equation method

In this section, we shall introduce a new type of vorticity–velocity method based on a space-time splitting of the problem that solves the time evolution of the vorticity as an ordinary differential equation on each node of the spatial discretization. The input for the vorticity transport equation at each time-step is computed from the spatial solution for the velocity field provided by a linear PDE expression in weak form called the *kinematic Laplacian equation* (henceforth referred to as KLE). The input of the KLE being provided by the time integration of the vorticity. The issue of the vorticity boundary conditions on the no-slip surface is dealt with by a sequence of two solutions of the KLE under a different set of velocity boundary conditions. Thus, inside each time step, we perform two projectional operations of integral character applied on the velocity field which ensures that the vorticity evolves in time in a way compatible with the time-dependent velocity boundary values.

2.1. The earlier form of the Laplacian approach: the constant-curl condition

In this section, we shall briefly describe some previous work which led to the development of the KLE. The initial motivation for the development of an approach to solve flow around bodies based on the Laplacian of the velocity field, as stated in [19], was to attain a mathematical expression that retains the simplicity and linearity of the potential-flow equation, but can also take into account rotational effects induced by a rotational component of the motion of a moving reference frame in which the analysis is performed. This roto-translational motion is typical of reference frames attached to moving bodies such as turbine blades, missiles and projectiles, manoeuvring aircraft and submarines, and dispersing seeds. It was originally intended to solve time-dependent no-separated flows around slender bodies. The idea is based on a kinematic scheme that, in this earlier form, states the vanishing of the Laplacian of the velocity field assuming incompressibility and constant curl. We start from the well-known vector identity:

$$\nabla^2 \boldsymbol{v} = \boldsymbol{\nabla} \cdot \boldsymbol{\nabla} \boldsymbol{v} = \boldsymbol{\nabla}(\boldsymbol{\nabla} \cdot \boldsymbol{v}) - \boldsymbol{\nabla} \times (\boldsymbol{\nabla} \times \boldsymbol{v}). \tag{1}$$

By incompressibility the first term on the right-hand side vanishes. Thus, if, furthermore, the curl of the velocity field is constant, the second term will also vanish, and we can obtain a solution for the velocity field by solving $\nabla^2 \boldsymbol{v} = 0$ using a standard Galerkin method under the constraints $\boldsymbol{\nabla} \cdot \boldsymbol{v} = 0$ and $\boldsymbol{\nabla} \times \boldsymbol{v} = \text{const.}$

This initial form, which was called the *constant-curl Laplacian equation* (henceforth CCLE) [19] assumes constant curl for the velocity field, and so is only valid so long as the boundary layer remains attached to the surface of the body. Consequently, its field of application is limited. Nevertheless, there are some real situations where these assumptions are fulfilled. For example, for wind turbine blades in normal operation and for other slender, streamlined bodies following curved trajectories the alignment of the incoming flow and the streamlined shape of the body prevents separation. The CCLE was successfully applied to the study of the aerodynamic behavior of wind turbines [20]. The Laplacian equation was intended to work within time-evolution schemes providing a quick, linear (but accurate if the assumptions are satisfied), spatial solution to the velocity field for successive time-steps.

2.2. The generalization of the Laplacian approach as a ($\boldsymbol{\omega}$, $\boldsymbol{v}$) method: the KLE

In order to overcome the limitations of the CCLE, we began to look for a generalized version that could handle separated flows and moving frames with angular acceleration. We found that a generalized form of the Laplacian expression (i.e., the KLE) could be advantageously used as the spatial counterpart of the vorticity transport equation in a new type of vorticity–velocity method.

Let us consider the full three-dimensional incompressible Navier–Stokes equation in vorticity form for a flow domain Ω with solid boundary $\partial\Omega$ and *external* boundary of Ω in the far field, in a moving frame of reference fixed to the solid,

$$\frac{\partial \boldsymbol{\omega}}{\partial t} = -\boldsymbol{v} \cdot \boldsymbol{\nabla}\boldsymbol{\omega} + \nu\nabla^2\boldsymbol{\omega} + \boldsymbol{\omega} \cdot \boldsymbol{\nabla}\boldsymbol{v}. \tag{2}$$

If we have the velocity field $\boldsymbol{v}$ in Ω at a certain instant of time, we can rewrite (2) as

$$\frac{\partial \boldsymbol{\omega}}{\partial t} = -\boldsymbol{v} \cdot \boldsymbol{\nabla}(\boldsymbol{\nabla} \times \boldsymbol{v}) + \nu\nabla^2(\boldsymbol{\nabla} \times \boldsymbol{v}) + (\boldsymbol{\nabla} \times \boldsymbol{v}) \cdot \boldsymbol{\nabla}\boldsymbol{v} \tag{3}$$

and solve for $\boldsymbol{\omega}$ at each point of the discretization of Ω by integration of (3) using an ODE solver.

Now, let us revisit (1) but this time impose a more general distribution for the vorticity field rather than just the constant curl condition:

$$\nabla^2\boldsymbol{v} = \boldsymbol{\nabla}\mathscr{D} - \boldsymbol{\nabla} \times \boldsymbol{\omega}, \tag{4}$$

$$\boldsymbol{\nabla} \cdot \boldsymbol{v} = \mathscr{D}, \tag{5}$$

$$\boldsymbol{\nabla} \times \boldsymbol{v} = \boldsymbol{\omega}. \tag{6}$$

Here, $\boldsymbol{\omega}$ is the vorticity field in Ω given by (3) and $\mathscr{D}$ is the corresponding rate of expansion (i.e., the divergence field). The KLE is essentially defined as a solution of (4) in its weak form under the simultaneous constraints (5) and (6).

For incompressible cases, such as discussed here, $\mathscr{D}$ is simply set to zero. For compressible cases, $\mathscr{D}$ can be a general distribution given by a solution analogous to (3) but for the divergence transport equation (i.e., the momentum equation in divergence form) together with a solution of the mass transport equation and adding to (2) and (3) the terms eliminated by the application of the incompressibility condition. We shall return to these ideas further on.

Now, provided that we can find a way of imposing on the velocity field the no-normal-flow condition

$$\boldsymbol{v} \cdot \boldsymbol{n} = 0 \tag{7}$$

and the no-slip condition,

$$\boldsymbol{v} \cdot \boldsymbol{\tau} = 0, \tag{8}$$

on the solid boundary $\partial\Omega$ in a way compatible with the vorticity distribution at that time, we obtain a compatible solution for the velocity. Then, from this velocity field, we produce the right-hand side of (3) required to advance the time-integration process to the next step. In order to impose the no-normal-flow and no-slip conditions on $\partial\Omega$ together with the correspondingly compatible boundary conditions on the vorticity, we designed a scheme based on two consecutive solutions of the KLE, which goes as follows:

(i) given a velocity field for the previous time-step $\boldsymbol{v}^{n-1}$ (which is compatible with the correspondent vorticity field $\boldsymbol{\omega}^{n-1}$), compute the next vorticity field $\tilde{\boldsymbol{\omega}}^n$ by time integration of (3) at each node of the spatial discretization. $\tilde{\boldsymbol{\omega}}^n$ is still incompatible with the velocity boundary conditions on the solid surface $\partial\Omega$;

(ii) get $\tilde{\boldsymbol{\omega}}_0^n$ by setting homogeneous conditions on $\partial\Omega$ for $\tilde{\boldsymbol{\omega}}^n$ (e.g., setting to zero the nodal values of $\tilde{\boldsymbol{\omega}}^n$ on $\partial\Omega$ once a discretization has been obtained);

(iii) compute a *free-slip* velocity field, $\vec{\boldsymbol{v}}^n$, by solving the KLE (i.e., solving (4) in its week form under the simultaneous constraints 5,6, with $\mathscr{D} = 0$). This solution uses $\tilde{\boldsymbol{\omega}}_0^n$ as input, applying only the no-normal-flow ($\boldsymbol{v} \cdot \boldsymbol{n} = 0$) condition on $\partial\Omega$ with the normal derivative of the tangential velocity set to zero;

(iv) from $\vec{v}^n$, compute the new vorticity field as $\boldsymbol{\omega}^n = \nabla \times \vec{v}^n$ applying both the no-normal-flow ($\boldsymbol{v} \cdot \boldsymbol{n} = 0$) and the no-slip condition ($\boldsymbol{v} \cdot \boldsymbol{\tau} = 0$) on $\partial\Omega$. Thus, $\boldsymbol{\omega}^n$ is a modified vorticity field produced in response to the induced slip which is compatible with the velocity boundary conditions on $\partial\Omega$;

(v) compute the final velocity field $\boldsymbol{v}^n$, by solving again the KLE but this time using $\boldsymbol{\omega}^n$ as input and applying both the no-normal-flow and the no-slip condition on $\partial\Omega$. In this way, $\boldsymbol{v}^n$ gives the weak solution for the velocity field at time-step n, which satisfies the time-dependent boundary conditions for the velocity, and simultaneously, its correspondent vorticity field $\boldsymbol{\omega}^n$ is compatible with those velocity boundary conditions.

In steps (iii)–(v), we apply the corresponding time-dependent, Dirichlet conditions for the velocity on $\partial\Omega_\infty$, the *external* boundary of Ω in the far field.

It is interesting to note that all the physics of the problem is contained in step (i) and it is solved as an ODE problem on the vorticity. Steps (ii)–(v) are concerned with the computation of a spatial solution for the velocity field which is compatible with both: the time-evolved vorticity distribution obtained in (i) and the time-dependent boundary conditions for the velocity. Setting homogeneous conditions on $\partial\Omega$ in step (ii) makes the vorticity field consistent with the *free-slip* solution of the velocity field to be computed in step (iii). Then, enforcing of the no-slip condition on $\partial\Omega$ in step (iv) gives the vorticity values in the boundary in response to the induced slip. This is the analog of the *vorticity-creation process* typically found in the early hybrid and nonprimitive methods mentioned above. Thus, we obtain our compatible vorticity boundary conditions on the solid surface by sequence of two solutions of the KLE under a different set of velocity boundary conditions. These two projectional operations of integral character applied on the velocity field (and performed inside each time step) ensure that the vorticity evolves in time in a way compatible with the time-dependent velocity boundary values. The algorithmic sequence defined in (i)–(v) is repeatedly performed inside the time-iteration process commanded by an adaptive variable-stepsize ODE solver. As we shall see later, we tested a predictor–corrector (ABM-PECE) solver and a fifth-order adaptive Runge–Kutta solver (see [21]). In both cases, solution is checked by the adaptive stepsize control by monitoring of local truncation error, which proved to be quite stable for this application.

The algorithmic sequence defined in (i)–(v) has the advantage of producing a complete decoupling between the time integration of the vorticity transport equation and the space solution of the Poisson equation for the velocity field. The linear spatial solution defined in (4)–(6) (i.e., the KLE) can be implemented in just one variational formulation. As we shall see later, this implementation leads to a global matrix which is independent both of time and of the particular constitutive relation of the continuum media. Then, this matrix can be factorized at the moment of assembling and its triangular factors used as many times as needed so long as we are using the same grid. As we said, this is so even for problems with different constitutive relations because all the physics of the problem is taken into account only in the time-integration process for the vorticity, i.e., the spatial solution is purely *kinematic*. Thus, the space solution performed at each time step reduces to a pair of back-substitution processes where we simply change the right-hand side vector of the linear system in order to impose consecutively the boundary conditions 7 and 8. This scheme simplifies the issue of obtaining the vorticity in order to satisfy the boundary conditions on the velocity. Note that it is not a purely local manipulation performed on the boundary, this double solution of the velocity field is calculated over the entire domain involving two projectional operations of nonlocal character.

2.3. Variational formulation for the KLE

To implement a variational formulation for the system (4)–(6) for the incompressible flow case, we start by applying the standard Galerkin method to (4):

$$\int_{\Omega} (\nabla \cdot \nabla \boldsymbol{v}) \cdot \boldsymbol{\delta v} \, \mathrm{d}\Omega = -\int_{\Omega} (\nabla \times \boldsymbol{\omega}) \cdot \boldsymbol{\delta v} \, \mathrm{d}\Omega, \tag{9}$$

where $\boldsymbol{\delta v}$ is an arbitrary, virtual velocity defined on Ω that vanishes on those sections of the boundary where Dirichlet conditions are applied. Then, integrating by parts and applying Gauss theorem, and taking into account that $\boldsymbol{\delta v}$ vanishes on $\partial\Omega_{\infty}$

$$\int_{\Omega} \nabla \boldsymbol{v} : \nabla \boldsymbol{\delta v} \, \mathrm{d}\Omega - \int_{\partial\Omega} \boldsymbol{n} \cdot \nabla \boldsymbol{v} \cdot \boldsymbol{\delta v} \, \mathrm{d}\Omega = \int_{\Omega} (\nabla \times \boldsymbol{\omega}) \cdot \boldsymbol{\delta v} \, \mathrm{d}\Omega. \tag{10}$$

Now, when the no-normal-flow and no-slip Dirichlet conditions are imposed on the solid boundary $\partial\Omega$ (step (v)), $\boldsymbol{\delta v}$ is zero then the second term of the first member of (10) vanishes. For the case of no-normal-flow and free-slip (step (iii)), just the normal component of $\boldsymbol{\delta v}$ is zero but the tangential components of $\boldsymbol{n} \cdot \nabla \boldsymbol{v}$ vanish due to free-slip. Hence, the second term of the first member of (10) is always zero, then

$$\int_{\Omega} \nabla \boldsymbol{v} : \nabla \boldsymbol{\delta v} \, \mathrm{d}\Omega = \int_{\Omega} (\nabla \times \boldsymbol{\omega}) \cdot \boldsymbol{\delta v} \, \mathrm{d}\Omega. \tag{11}$$

One important property of the Laplacian operator is that its variational formulation yields a symmetric and coercive bilinear form with good stability and convergence properties, and it has an equivalent minimization formulation with associated functional

$$\Phi = \int_{\Omega} \frac{1}{2} \nabla \boldsymbol{v} : \nabla \boldsymbol{v} \, \mathrm{d}\Omega - \int_{\Omega} (\nabla \times \boldsymbol{\omega}) \cdot \boldsymbol{v} \, \mathrm{d}\Omega. \tag{12}$$

The next step is the imposition of the constraints 5 and 6. To this end, we explored several alternatives: an augmented Lagrangian scheme, a Lagrangian multiplier mixed formulation and the penalty method. As the kinematic Laplacian equation is intended to be applied successively in time, we discarded the augmented Lagrangian option because its iterative nature would imply that one had to nest one loop within another, and this would increase the computational cost. In our tests on this particular application the Lagrangian multiplier formulation did not appear to show a drastic improvement compared to the penalty method, and it affects the positive definiteness of the final bilinear form. On the other hand, in normal application solving the momentum equation in primitive variables, the multiplier itself is associated to the value of the pressure field, but for the KLE case, it has no physical meaning at all but is just an auxiliary variable that does not give us any additional information. Nevertheless, with a view to future applications we intend to conduct further exploration of a possible mixed formulation in the context of the finite element method, based on discontinuous interpolation of the auxiliary variables combined with their condensation at elementary level. The penalty method, though less rigorous than the alternatives with regard to the imposition of constraints, appears very well suited to this new approach. It provides a solution in one step, it keeps the positive definiteness of the final bilinear form, it has proven to work properly in this coupled scheme of two simultaneous constraints, it shows a wide range of stability for the values of the penalty constant used to impose the constraints without inducing ill-conditioning on the final stiffness matrix, as we shall see later, it produces results that are in good agreement with experiments. Thus, we finally settled on the penalty method for the imposition of the constraints, and we modified the functional (12) by adding the penalty terms related to the constraints 5 and 6

$$\tilde{\Phi} = \Phi + \int_{\Omega} \frac{\alpha_{\mathscr{D}}}{2} (\nabla \cdot \boldsymbol{v})^2 + \frac{\alpha_{\omega}}{2} (\nabla \times \boldsymbol{v} - \boldsymbol{\omega}) \cdot (\nabla \times \boldsymbol{v} - \boldsymbol{\omega}) \mathrm{d}\Omega, \tag{13}$$

where $\tilde{\Phi}$ is the modified functional and $\alpha_{\mathscr{D}}$ and α_{ω} the corresponding penalty constants. We satisfactorily tested values of $\alpha_{\mathscr{D}}$ from 10^2 to 10^5 (choosing 10^3) and values of α_{ω} from 10^1 to 10^6 (choosing 10^2).

Invoking the stationarity of $\tilde{\Phi}$ with respect to $\boldsymbol{v}$,

$$\delta\tilde{\Phi} = \int_\Omega \nabla\boldsymbol{v} : \nabla\boldsymbol{\delta v} - (\nabla\times\boldsymbol{\omega})\cdot\boldsymbol{\delta v} + \alpha_{\mathscr{D}}(\nabla\cdot\boldsymbol{v})(\nabla\cdot\boldsymbol{\delta v}) + \alpha_{\omega}(\nabla\times\boldsymbol{v}-\boldsymbol{\omega})\cdot(\nabla\times\boldsymbol{\delta v})\,\mathrm{d}\Omega = 0. \tag{14}$$

Reordering the terms, we finally have

$$\int_\Omega \nabla\boldsymbol{v} : \nabla\boldsymbol{\delta v} + \alpha_{\mathscr{D}}(\nabla\cdot\boldsymbol{v})(\nabla\cdot\boldsymbol{\delta v}) + \alpha_{\omega}(\nabla\times\boldsymbol{v})\cdot(\nabla\times\boldsymbol{\delta v})\,\mathrm{d}\Omega = \int_\Omega (\nabla\times\boldsymbol{\omega})\cdot\boldsymbol{\delta v} + \alpha_{\omega}\boldsymbol{\omega}\cdot(\nabla\times\boldsymbol{\delta v})\mathrm{d}\Omega, \tag{15}$$

which is the expression for the variational formulation corresponding to the system (4)–(6) for the incompressible flow case.

3. Numerical implementation of the KLE method

In this section, we shall describe the first numerical implementation of the KLE method using the finite element method (FEM) for the spatial discretization and a predictor–corrector ODE solver for time integration. Those particular techniques were chosen for their convenience to the particular problems we were dealing with. Nevertheless, other discretization techniques may be applied to the implementation of the KLE method and we plan to explore different options in the future. In what follows, classical FEM techniques are described for interpolation, integration, imposition of constraints and boundary conditions, and calculation of derivatives; a comprehensive treatment of them can be found in [22,23].

3.1. Finite element implementation of the spatial solution

For the discretization of (15) in two-dimensional applications we used nine-node biquadratic isoparametric finite elements, which though "expensive" in computational terms possess a high convergence rate and, due their biquadratic interpolation of the geometric coordinates, provide the additional ability of reducing the so-called skin-error on curvilinear boundaries when compared to linear elements. Fig. 1 shows the biquadratic interpolation functions (h^k, $k = 1,\ldots,9$) of the nine-node isoparametric element on its

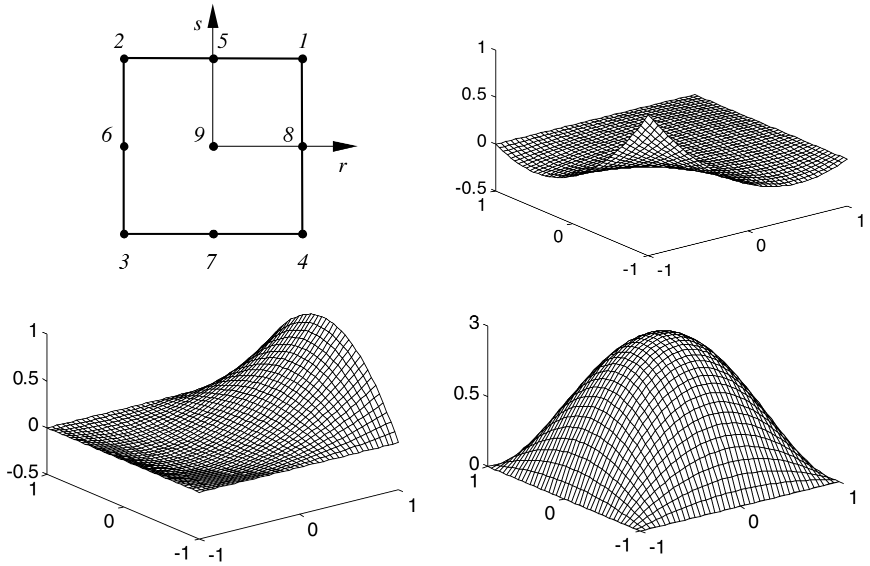

Fig. 1. Interpolation functions of the nine-node isoparametric element showing its natural system of coordinates, node numeration and three examples of functions: for a corner node (node 3), for a central-lateral node (node 8) and for the central node (node 9).

natural system of coordinates (r, s) (for a detailed description of the isoparametric-element technique and its corresponding interpolation functions see [22]).

Following the standard procedure for finite element discretization of the velocity field and its gradient we have

$$\boldsymbol{v} = \begin{bmatrix} v_x \\ v_y \end{bmatrix} = \boldsymbol{H} \cdot \hat{\boldsymbol{V}}^{\boldsymbol{e}}, \quad \nabla \boldsymbol{v} = \begin{bmatrix} \frac{\partial v_x}{\partial x} \\ \frac{\partial v_x}{\partial y} \\ \frac{\partial v_y}{\partial x} \\ \frac{\partial v_y}{\partial y} \end{bmatrix} = \boldsymbol{B} \cdot \hat{\boldsymbol{V}}^{\boldsymbol{e}}, \tag{16}$$

where $\hat{\boldsymbol{V}}^{\boldsymbol{e}}$ is the nine-node elemental array of nodal velocity values, $\boldsymbol{H}$ is the interpolation-function array and B the array of interpolation-function derivatives,

$$\hat{\boldsymbol{V}}^{\boldsymbol{e}} = \begin{bmatrix} \hat{v}_x^1 \\ \hat{v}_y^1 \\ \hat{v}_x^2 \\ \vdots \\ \hat{v}_x^9 \\ \hat{v}_y^9 \end{bmatrix}, \quad \boldsymbol{H} = \begin{bmatrix} h^1 & 0 & h^2 & \cdots & h^9 & 0 \\ 0 & h^1 & 0 & \cdots & 0 & h^9 \end{bmatrix}, \tag{17}$$

$$\boldsymbol{B} = \begin{bmatrix} \frac{\partial h^1}{\partial x} & 0 & \frac{\partial h^2}{\partial x} & \cdots & \frac{\partial h^9}{\partial x} & 0 \\ \frac{\partial h^1}{\partial y} & 0 & \frac{\partial h^2}{\partial y} & \cdots & \frac{\partial h^9}{\partial y} & 0 \\ 0 & \frac{\partial h^1}{\partial x} & 0 & \cdots & 0 & \frac{\partial h^9}{\partial x} \\ 0 & \frac{\partial h^1}{\partial y} & 0 & \cdots & 0 & \frac{\partial h^9}{\partial y} \end{bmatrix}. \tag{18}$$

The partial derivatives of the interpolation functions are given by

$$\begin{bmatrix} \frac{\partial h^k}{\partial x} \\ \frac{\partial h^k}{\partial y} \end{bmatrix} = \boldsymbol{J}^{-1} \cdot \begin{bmatrix} \frac{\partial h^k}{\partial r} \\ \frac{\partial h^k}{\partial s} \end{bmatrix}, \quad k = 1, \ldots, 9, \tag{19}$$

where $\boldsymbol{J}$ is the elemental Jacobian matrix,

$$\boldsymbol{J} = \begin{bmatrix} \sum_{k=1}^{9} \frac{\partial h^k}{\partial r} \hat{x}^k & \sum_{k=1}^{9} \frac{\partial h^k}{\partial r} \hat{y}^k \\ \sum_{k=1}^{9} \frac{\partial h^k}{\partial s} \hat{x}^k & \sum_{k=1}^{9} \frac{\partial h^k}{\partial s} \hat{y}^k \end{bmatrix} \tag{20}$$

and ($\hat{x}^k$, $\hat{y}^k$) the geometrical coordinates of the nodes. For the divergence of the velocity field, we have

$$\nabla \cdot \boldsymbol{v} = \boldsymbol{m} \cdot \boldsymbol{B} \cdot \hat{\boldsymbol{V}}^{\boldsymbol{e}}, \quad \boldsymbol{m} = [1 \quad 0 \quad 0 \quad 1], \tag{21}$$

and for the velocity curl,

$$\nabla \times \boldsymbol{v} = \boldsymbol{r} \cdot \boldsymbol{B} \cdot \hat{\boldsymbol{V}}^{\boldsymbol{e}}, \quad \boldsymbol{r} = [0 \quad -1 \quad 1 \quad 0]. \tag{22}$$

Following a similar procedure for the discretization of the vorticity field and its curl, we have

$$\boldsymbol{\omega} = \omega = \boldsymbol{H}_\omega \cdot \hat{\boldsymbol{\omega}}^{\boldsymbol{e}}, \quad \nabla \times \boldsymbol{\omega} = \begin{bmatrix} \frac{\partial \omega}{\partial y} \\ -\frac{\partial \omega}{\partial x} \end{bmatrix} = \boldsymbol{B}_\omega \cdot \hat{\boldsymbol{\omega}}^{\boldsymbol{e}}, \tag{23}$$

where $\hat{\boldsymbol{\omega}}^e$ is the nine-node elemental array of nodal vorticity values provided by the time-integration process, $\boldsymbol{H}_\omega$ is the vorticity interpolation-function array and $\boldsymbol{B}_\omega$ the array of interpolation-function derivatives for the computation of the vorticity curl,

$$\hat{\boldsymbol{\omega}}^e = \begin{bmatrix} \hat{\omega}^1 \\ \hat{\omega}^2 \\ \vdots \\ \hat{\omega}^9 \end{bmatrix}, \quad \boldsymbol{H}_\omega = \begin{bmatrix} h^1 & h^2 & \cdots & h^9 \end{bmatrix}, \tag{24}$$

$$\boldsymbol{B}_\omega = \begin{bmatrix} \frac{\partial h^1}{\partial y} & \frac{\partial h^2}{\partial y} & \cdots & \frac{\partial h^9}{\partial y} \\ -\frac{\partial h^1}{\partial x} & -\frac{\partial h^2}{\partial x} & \cdots & -\frac{\partial h^9}{\partial x} \end{bmatrix}. \tag{25}$$

Now, considering (15) at each elemental subdomain (Ω^e) and substituting the velocity and vorticity fields and their differentiated magnitudes by their discretized counterparts, we have

$$\boldsymbol{\delta}\hat{\boldsymbol{V}}^{e\mathrm{T}} \cdot \underbrace{(\boldsymbol{K}_L^e + \boldsymbol{K}_{\mathscr{D}}^e + \boldsymbol{K}_\omega^e)}_{\boldsymbol{K}^e} \cdot \hat{\boldsymbol{V}}^e = \boldsymbol{\delta}\hat{\boldsymbol{V}}^{e\mathrm{T}} \cdot \underbrace{(\boldsymbol{R}_L^e + \boldsymbol{R}_\omega^e)}_{\boldsymbol{R}^e} \cdot \hat{\boldsymbol{\omega}}^e, \tag{26}$$

where

$$\boldsymbol{K}_L^e = \int_{\Omega^e} \boldsymbol{B}^\mathrm{T} \cdot \boldsymbol{B} \mathrm{d}\Omega = \int_{-1}^{1} \int_{-1}^{1} \boldsymbol{B}^\mathrm{T} \cdot \boldsymbol{B} |\boldsymbol{J}| \,\mathrm{d}r \,\mathrm{d}s, \tag{27}$$

$$\boldsymbol{K}_{\mathscr{D}}^e = \int_{-1}^{1} \int_{-1}^{1} \alpha_{\mathscr{D}} \boldsymbol{B}^\mathrm{T} \cdot \boldsymbol{m}^\mathrm{T} \cdot \boldsymbol{m} \cdot \boldsymbol{B} |\boldsymbol{J}| \,\mathrm{d}r \,\mathrm{d}s, \tag{28}$$

$$\boldsymbol{K}_\omega^e = \int_{-1}^{1} \int_{-1}^{1} \alpha_\omega \boldsymbol{B}^\mathrm{T} \cdot \boldsymbol{r}^\mathrm{T} \cdot \boldsymbol{r} \cdot \boldsymbol{B} |\boldsymbol{J}| \,\mathrm{d}r \,\mathrm{d}s, \tag{29}$$

$$\boldsymbol{R}_L^e = \int_{-1}^{1} \int_{-1}^{1} \boldsymbol{H}^\mathrm{T} \cdot \boldsymbol{B}_\omega |\boldsymbol{J}| \,\mathrm{d}r \,\mathrm{d}s, \tag{30}$$

$$\boldsymbol{R}_\omega^e = \int_{-1}^{1} \int_{-1}^{1} \alpha_\omega \boldsymbol{B}^\mathrm{T} \cdot \boldsymbol{r}^\mathrm{T} \cdot \boldsymbol{H}_\omega |\boldsymbol{J}| \,\mathrm{d}r \,\mathrm{d}s, \tag{31}$$

and $\boldsymbol{\delta}\hat{\boldsymbol{V}}^e$ is the elemental array of nodal values for the arbitrary function $\boldsymbol{\delta v}$. The integrals involved in (27) and (30) were solved by 3 × 3 Gaussian integration which is recommended for the biquadratic interpolation used by nine-node isoparametric elements. For the integrals in (28), (29) and (31), we used 2 × 2 Gaussian reduced integration which is recommended for the imposition of constraints in order to avoid locking problems. A comprehensive treatment of this subject can be found in [22].

Assembling the elemental matrices and arrays defined in (26) and taking into account that $\boldsymbol{\delta v}$ is arbitrary and so it is its discretized counterpart $\boldsymbol{\delta}\hat{\boldsymbol{V}}$, we arrive to the global system

$$\boldsymbol{K} \cdot \hat{\boldsymbol{V}} = \boldsymbol{R} \cdot \hat{\boldsymbol{\omega}}. \tag{32}$$

In order to combine the power of convergence of the nine-node quadrilateral isoparametric element with the geometrical ability of a triangular grid to create suitable nonstructured meshes with gradual and smooth changes of density, we implemented what we called tri-quadrilateral isoparametric elements [19,20]. The tri-quadrilateral elements consist of an assembling of three quadrilateral nine-nod isoparametric elements

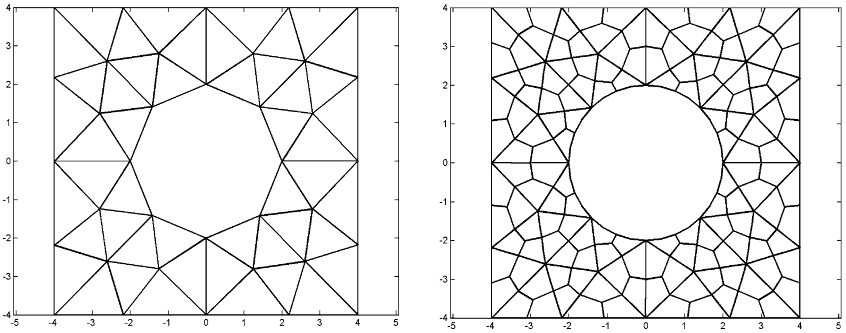

Fig. 2. An example of a mesh of tri-quadrilateral finite elements obtained from a standard triangular discretization.

in which each triangle of a standard unstructured mesh is divided into. Fig. 2 shows a schematic example of a mesh of tri-quadrilateral finite elements obtained from the original triangular discretization.

Another advantage of the tri-quadrilateral scheme is that, by a previous condensation of the nodes that lie inside the triangle, we can significantly reduce the number of nodes to solve in the final system, subsequently recovering the values for the internal nodes from the solution on the noncondensable nodes. Fig. 3 shows a schematic view of the internal topology of the tri-quadrilateral element including the in-triangle global numeration of the nodes and indicating the three nine-node subelements (I)–(III).

The internal nodes 13–19 may be expressed in terms of nodes 1–12 which lay on the elemental boundary. Following the classical procedure for elemental condensation (see [22]), we rewrite the system $\boldsymbol{K}^e \cdot \hat{\boldsymbol{V}}^e = \boldsymbol{R}^e \cdot \hat{\omega}^e$

$$\begin{bmatrix} \boldsymbol{K}^e_{aa} & \boldsymbol{K}^e_{ab} \\ \boldsymbol{K}^e_{ba} & \boldsymbol{K}^e_{bb} \end{bmatrix} \cdot \begin{bmatrix} \hat{\boldsymbol{V}}^e_a \\ \hat{\boldsymbol{V}}^e_b \end{bmatrix} = \begin{bmatrix} \boldsymbol{R}^e_a \\ \boldsymbol{R}^e_b \end{bmatrix} \cdot \hat{\omega}^e, \tag{33}$$

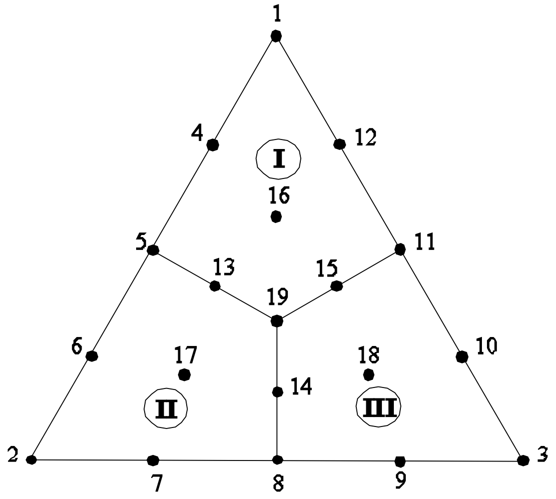

Fig. 3. Schematic view of the internal topology of the tri-quadrilateral element. Subelements (I)–(III) are model by standard nine-node isoparametric interpolation. Numbers 1–19 indicate the in-triangle nodal numeration.

where subindex a indicates the velocity degrees of freedom 1–24 associated with nodes 1–12 and subindex b the velocity degrees of freedom 25–38 associated with nodes 13–19. From the second row of (33), we have,

$$\hat{\boldsymbol{V}}^e_b = \underbrace{(\boldsymbol{K}^e_{bb})^{-1}\cdot\boldsymbol{R}^e_b}_{\tilde{\boldsymbol{R}}^e_b}\cdot\hat{\boldsymbol{\omega}}^e - \underbrace{(\boldsymbol{K}^e_{bb})^{-1}\cdot\boldsymbol{K}^e_{ba}}_{\tilde{\boldsymbol{K}}^e_{ba}}\cdot\hat{\boldsymbol{V}}^e_a, \tag{34}$$

substituting this result into the first row of (33) and reordering the terms,

$$\underbrace{\left(\boldsymbol{K}^e_{aa} - \boldsymbol{K}^e_{ab}\cdot(\boldsymbol{K}^e_{bb})^{-1}\cdot\boldsymbol{K}^e_{ba}\right)}_{\tilde{\boldsymbol{K}}^e}\cdot\hat{\boldsymbol{V}}^e_a = \underbrace{\left(\boldsymbol{R}^e_a - \boldsymbol{K}^e_{ab}\cdot(\boldsymbol{K}^e_{bb})^{-1}\cdot\boldsymbol{R}^e_b\right)}_{\tilde{\boldsymbol{R}}^e}\cdot\hat{\boldsymbol{\omega}}^e, \tag{35}$$

which defines the new condensed system to solve. Assembling the elemental matrices and arrays defined in (34) and (35), we finally arrive to the global condensed system

$$\tilde{\boldsymbol{K}}\cdot\hat{\boldsymbol{V}}_a = \tilde{\boldsymbol{R}}\cdot\hat{\boldsymbol{\omega}}, \tag{36}$$

$$\hat{\boldsymbol{V}}_b = \tilde{\boldsymbol{R}}_b\cdot\hat{\boldsymbol{\omega}} - \tilde{\boldsymbol{K}}_{ba}\cdot\hat{\boldsymbol{V}}_a, \tag{37}$$

which gives the solution for the complete velocity field $\hat{\boldsymbol{V}}$. This process of condensation allows us to reduce the size of the system to solve in (36) to approximately a 40% of the original system (32). Neither $\tilde{\boldsymbol{K}}, \tilde{\boldsymbol{R}}, \tilde{\boldsymbol{R}}_b$ nor $\tilde{\boldsymbol{K}}_{ba}$ depend on $\hat{\boldsymbol{\omega}}$ nor t, so they can be computed once for a given mesh, stored and used as many times as needed to compute the solution for $\hat{\boldsymbol{V}}$. Matrix $\tilde{\boldsymbol{K}}$ is symmetric and positive definite, so it lends to factorization by Cholesky decomposition and its triangular factor is repeatedly used to solve $\hat{\boldsymbol{V}}_a$ through back-substitution.

3.2. Time integration of the vorticity transport equation

For the implementation of the time-integration procedure, we rewrite the two-dimensional vorticity transport equation in a more convenient way

$$\frac{\partial\boldsymbol{\omega}}{\partial t} = \boldsymbol{F}(\boldsymbol{\omega}, t) = \nabla\times(\nu\nabla\cdot\nabla\boldsymbol{v} - \boldsymbol{v}\cdot\nabla\boldsymbol{v}), \tag{38}$$

We evaluate the right-hand side of (38) applying the corresponding differential operators onto the discrete velocity field $\hat{\boldsymbol{V}}$ calculated following steps (ii)–(v) in Section (2.2). The normal procedure to calculate derivatives on the nodes of a mesh of isoparametric elements consists in computing the derivatives in the Gaussian points adjacent to each node and interpolate their results following several alternatives techniques. A detailed description of the this procedure can be found in [22]. In our case, we used area-weighing interpolation which prove to be very effective. The contribution of each Gaussian point to its corresponding node depends on the constitution of the mesh and can be calculated at the moment of assembling. A set of arrays that perform the differential operations is assembled simultaneously with the finite element matrices and the right-hand side of (38) takes the form,

$$\boldsymbol{F}(\hat{\boldsymbol{\omega}}, t) = \hat{\boldsymbol{C}}_{\text{url}}\cdot\left(\nu\hat{\boldsymbol{D}}_{\text{iv}} - \hat{\boldsymbol{V}}_{\text{adv}}\right)\cdot\hat{\boldsymbol{G}}_{\text{rad}}\cdot\hat{\boldsymbol{V}}, \tag{39}$$

where $\hat{\boldsymbol{C}}_{\text{url}}$, $\hat{\boldsymbol{G}}_{\text{rad}}$ and $\hat{\boldsymbol{D}}_{\text{iv}}$ are, respectively, the arrays that compute the curl, the gradient and the divergence of the gradient, and $\hat{\boldsymbol{V}}_{\text{adv}}$ is simply a reordering of $\hat{\boldsymbol{V}}$ array to perform the product $\boldsymbol{v}\cdot\nabla\boldsymbol{v}$ in the advective term.

Neither $\hat{\boldsymbol{C}}_{\text{url}}$, $\hat{\boldsymbol{G}}_{\text{rad}}$ nor $\hat{\boldsymbol{D}}_{\text{iv}}$ depend on $\hat{\boldsymbol{\omega}}$ nor t, so they can also be computed once for a given mesh, stored and used as many times as needed to provide evaluation of (38) right-hand side for an advanced package ODE solver. We choose a multivalue variable-order Adams–Bashforth–Moulton predictor–corrector

(ABM-PECE) solver with adaptive stepsize control which proved to be quite efficient for this application. We also tried a fifth order adaptive-stepsize Runge–Kutta algorithm with good results. For the first DNS low-Reynolds-number applications of the KLE method, the function prove to be smooth enough for the adaptive ABM-PECE algorithm to work very efficiently, in these smooth cases the predictor–corrector outperforms other alternatives like the Bulirsch–Stoer method [21]. We shall discuss some future options for the time-integration process further on.

4. Validation test

This section describes a validation test of the KLE method against the well-known problem of a semi-infinite region of stationary fluid bounded by an infinite horizontal flat plate at $y = 0$, which is suddenly given a velocity U in its own plane and thereafter maintained at that speed. This problem has an exact analytic solution (see [24], Section 4.3, among others). The normalized velocity field described in a frame of reference fixed to a plate moving in the $-x$ direction is

$$\frac{u(y,t)}{U} = \mathrm{erf}\left(\frac{y}{\sqrt{4\nu t}}\right), \tag{40}$$

where erf is the error function and y is the vertical coordinate. Fig. 4 shows a comparison between the numerical results given by the KLE method for the velocity profile at successive values of the parameter $\tau = \sqrt{4\nu t}$ and the correspondent exact solution given by (40). These results are in good agreement with the exact solution lending confidence to the accuracy of the numerical simulations. This problem is closely related with the key process of the KLE method, i.e., the vorticity production at a solid surface due to the induced slip and its further propagation to the body of the fluid.

This validation test was repeatedly performed for a succession of uniformly-distributed unstructured meshes, progressively refined, and the max-norm and mean-norm of the error was evaluated. Fig. 5 shows the evolution of the error in function of the number of nodes, and Fig. 6 shows the evolution of the error in function of the average value of the time-step.

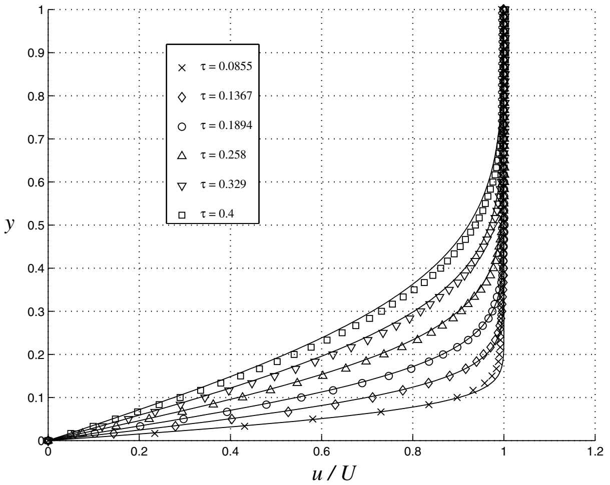

Fig. 4. A comparison between the numerical results given by the KLE method for the velocity profile at successive values of the parameter $\tau = \sqrt{4\nu t}$ and the correspondent exact solution given by (40).

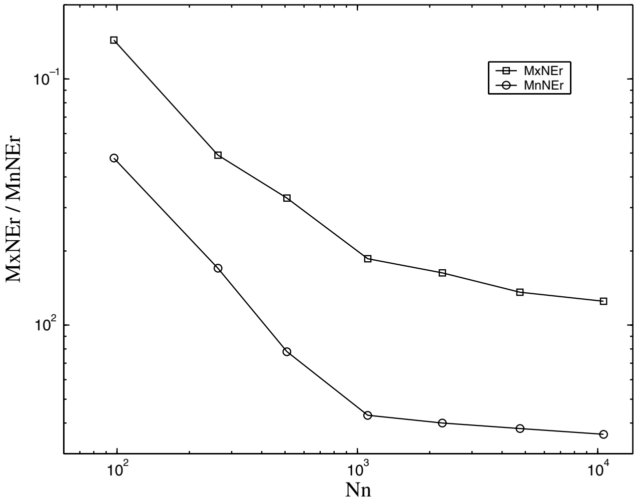

Fig. 5. Evolution of the max-norm (MxNEr) and mean-norm (MnNEr) of the velocity error in function of the number of nodes (Nn) of the uniformly-distributed test mesh.

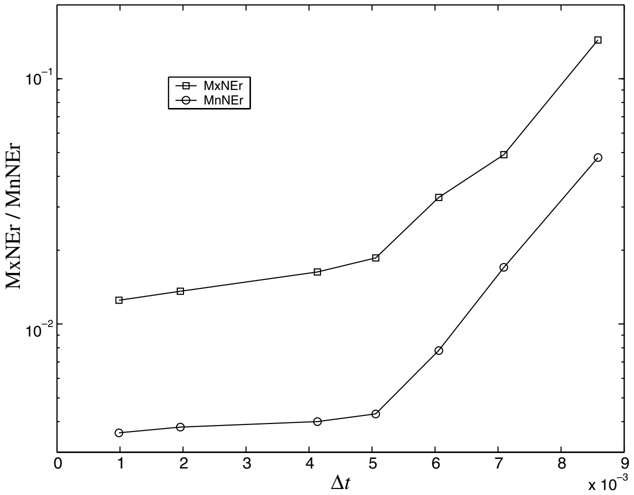

Fig. 6. Evolution of the max-norm (MxNEr) and mean-norm (MnNEr) of the velocity error in function of the average time-step (Δt).

5. Some examples of application of the KLE method

We first show some results produced by the KLE method for the well-studied case of a circular cylinder started impulsively and then subjected to steady translational motion through fluid otherwise at rest. Fig. 7 shows an example of a mesh of tri-quadrilateral elements used.

We shall see results at several values of Reynolds number, $Re = Ud/v$, where U is the horizontal translational speed of the cylinder, d its diameter, and v the kinematic viscosity of the fluid. Fig. 8 shows a sequence plot of the vorticity isolines during one cycle of the vortex-shedding process in the wake of a circular cylinder in steady motion at $Re = 140$ superimposed onto an arrow plot of the solenoidal

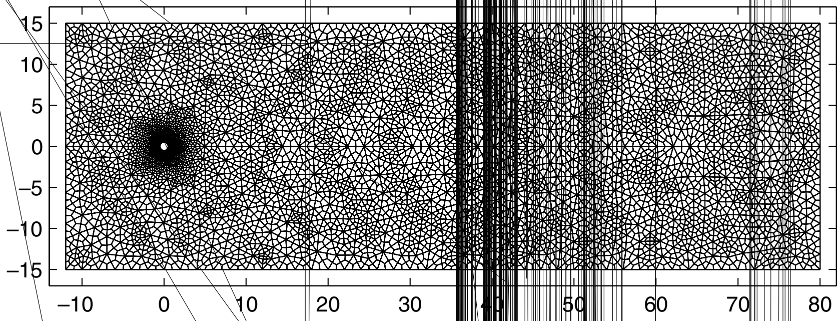

Fig. 7. An example of a mesh of tri-quadrilateral finite elements used for the present analysis (geometrical coordinates are given in diameters).

component of the velocity field $\boldsymbol{v}_{\omega}$. Starting at the bottom-left panel, and following the sequence clockwise to complete the cycle, it is possible to follow the evolution of the vorticity as it interacts with the eddy-structures defined by the streamlines of $\boldsymbol{v}_{\omega}$. Fig. 9 shows a close-up of the same images where we can see the rolling-up of the shear layers around the eddy-structures in $\boldsymbol{v}_{\omega}$ at the early stages of vortex-formation.

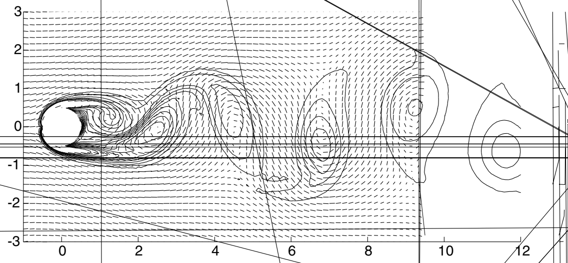

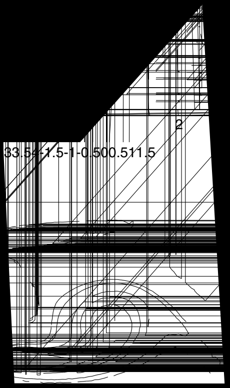

ge
oint
clas-
Fig. 11.

hind a trans-
to Zdravkovich
Reynolds number.
appear clear while
and the magnitude of

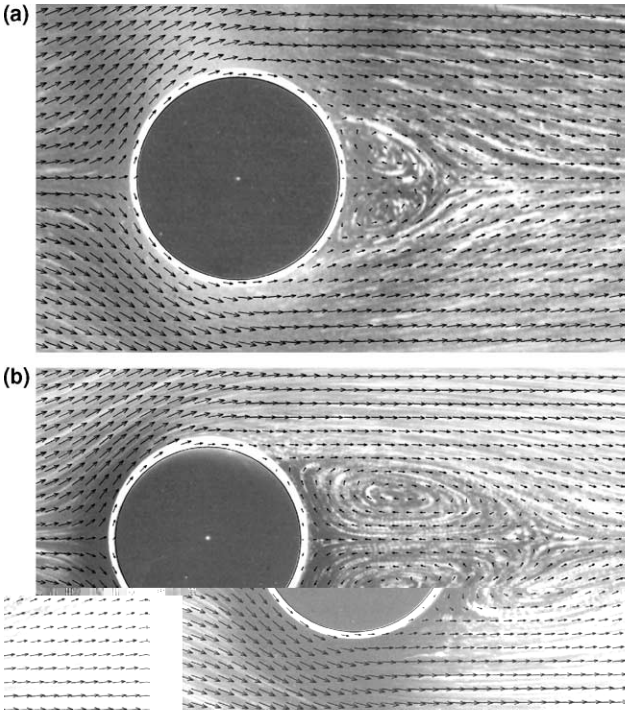

Fig. 10. Comparison of flow visualizations by Taneda and arrow-plots from numerical results for the twin-vortex wake behind a cylinder at (a) $Re = 13.05$ and (b) $Re = 26$.

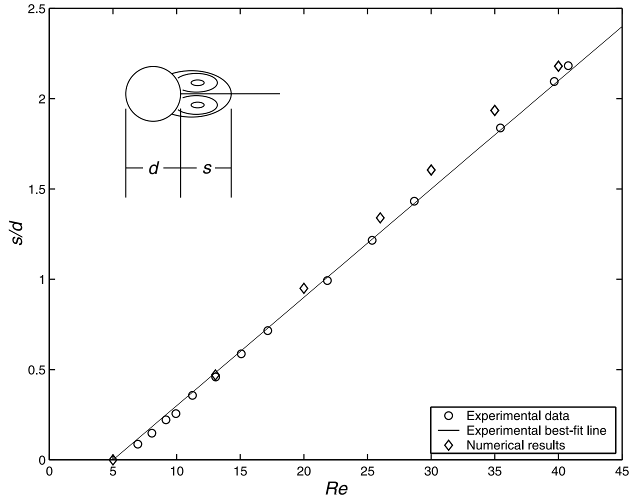

Fig. 11. Comparison of the wake length calculated by the kinematic Laplacian equation method and the experimental measurements by Taneda [26].

vorticity displayed from the computation are, of course, not the same. Nevertheless, the correspondence in the spacing, and even the shape of the vortices, lends considerable confidence to the fidelity of the numerical simulations.

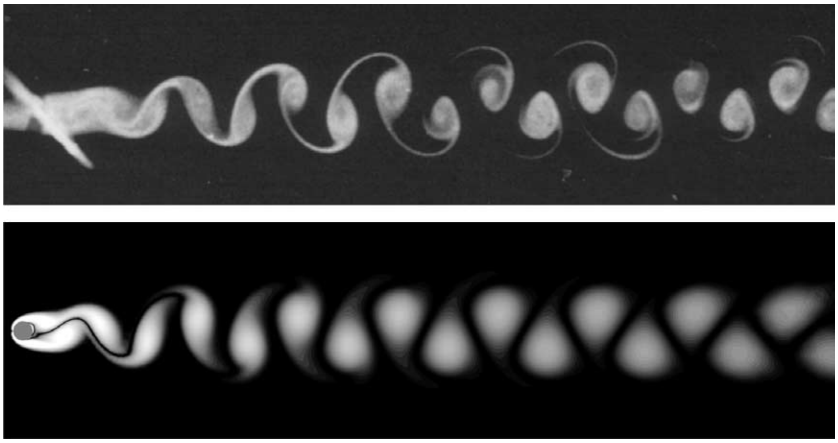

Fig. 12. Comparison of flow visualization of a Kármán vortex street behind a cylinder at $Re = 100$ by Zdravkovich with a gray scale plot of the vorticity field produced by the kinematic Laplacian equation method at the same value of Reynolds number.

As our third test case, we measured the dominant frequency, f, of vorticity fluctuations at a set of points in the vortex street wake for the range of Reynolds numbers $50 < Re < 180$, and we computed the corresponding value of the Strouhal number ($St = fd/U$). The dominant frequency is the same for all the points probed, and it is clearly defined at an early stage of wake formation. The amplitude of the fluctuations, on the other hand, displays a transient state until it reaches its final, constant value somewhat downstream. Plotting St vs. Re, as shown in Fig. 13, compares very favorably with the experiments presented by Williamson [27].

Finally, we have recently started a study on the formation, shedding and further evolution of periodic vortex-array structures produced in the wake of forced-oscillating cylinders. Several qualitatively distinct wake regimes were observed experimentally depending on the wavelength of the undulatory motion of

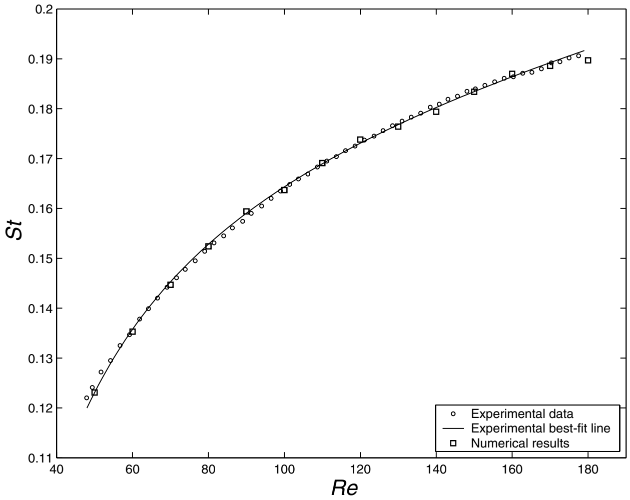

Fig. 13. Comparison of the Strouhal number calculated by the kinematic Laplacian equation method and the experimental measurements by Williamson [27] for $Re < 180$.

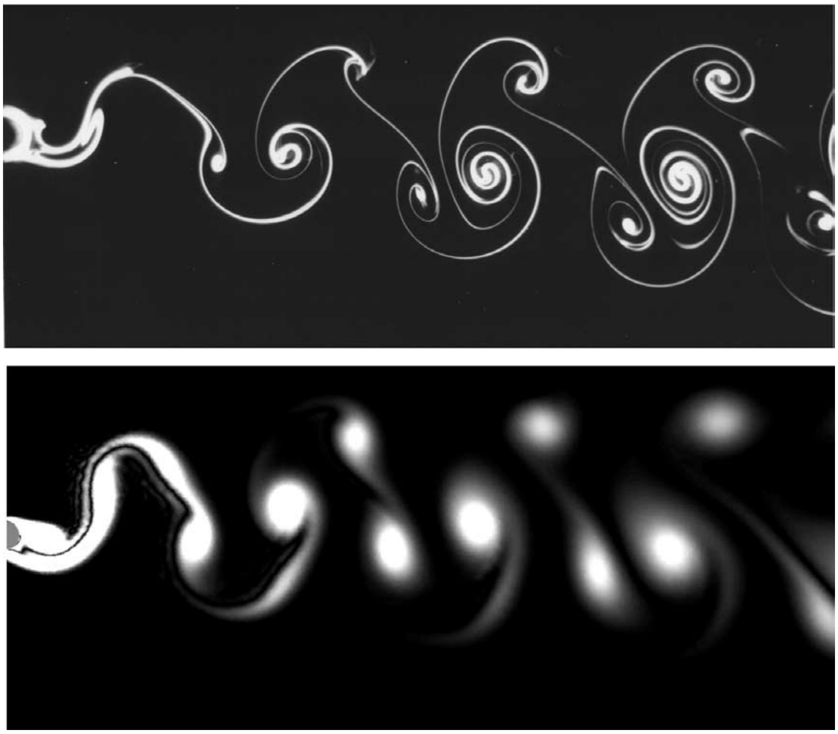

Fig. 14. Comparison of flow visualization of a P + S wake of an oscillating cylinder for *Re* = 140 by Williamson (private communication to H. Aref) with a gray scale plot of the vorticity field produced by the KLE method at the same Reynolds number.

the cylinder and the amplitude of the transverse undulations. For instance, for a certain range in the combination of the wavelength/amplitude parameters, a pattern in which one pair and a single vortex are shed in each cycle of the forced oscillation is produced. This pattern is commonly know as P + S (one pair plus one single vortex). Fig. 14 shows a comparison of a gray scale plot of the vorticity field calculated by the KLE method with an experimental laser-fluorescene photograph for an oscillating cylinder at *Re* = 140. This photo was kindly provided by Prof. Williamson.

6. Concluding remarks and future prospects

We have introduced a mathematical-computational approach to solve the time-dependent flow in a non-inertial frame of reference attached to a body in translational and/or roto-translational motion. The KLE method was validated for two-dimensional DNS applications against experimental results for incompressible flow around circular cylinders at low Reynolds number, finding very good agreement.

The basic formulation of the PDE system (4)–(6), i.e., the KLE, is three-dimensional. Then, the extension of the spatial solution provided by the KLE to three-dimensional problems is relatively straightforward. The theoretical basis of the vorticity–velocity formulation in three dimensions can be found in Quartapelle [1], Chapter 4. In Quartapelle's study, a series of theorems proves the equivalence between the $(\boldsymbol{\omega}, \boldsymbol{v})$ formulation of the incompressible Navier–Stokes equations and their classical velocity–pressure formulation. Hence, the main issue to deal with in a future three-dimensional implementation of the KLE method is the algorithmic sequence to get a velocity field compatible with the vorticity boundary conditions.

The fact that the velocity is supplemented by unique boundary conditions, simplifies this question substantially. Contrarily, with the vorticity-stream function methods, the variety of boundary conditions that can be chosen for the velocity potentials due to the nonuniqueness of the velocity representation is much more complicated in three-dimensions than in two.

The KLE method has no special requirements on the rate-of-expansion distribution which is imposed. It implies that the method can be extended to the analysis of compressible flows, provided that we find a way of dealing with compatible boundary conditions for the rate-of-expansion in an analog way as we do with the vorticity.

Since it is a new approach, we are still exploring KLE method capabilities to manage higher Reynolds-number flows in DNS, and its potential to be extended to LES applications. The fact that the linear spatial solution provided by the KLE is purely kinematic with all the nonlinearities and the material constitutive properties remitted to the high-order adaptive time integration, favors the solution of problems with more complex constitutive relations like non-Newtonian, plastic or viscoplastic flows. And the same argument may be applied to the adoption of turbulence models for a future LES implementation of the method.

The KLE is based on a universal vectorial relation, so it can be used to solved any vector field provided that we can solve a transport equation for its divergence and curl. This together with the fact that time is the only iteration variable present, makes it possible to extend its application to other physical problems like electromagnetic fields. It is also possible to couple the fluid analysis with other physical processes (e.g., heat transfer or chemical reaction) by adding more equations to the ODE system, using grids with different densities for problems with different scales.

Regarding the numerical implementation of the KLE method, the techniques mentioned above: Cholesky decomposition/back-substitution for the spatial solution and adaptive predictor–corrector solver for time integration, prove to be very efficient for a two-dimensional low Reynolds number implementation of the method in a sequential code. In view to solve problems in complex geometries in three-dimensional applications which will require a substantial number of nodes (leading to large sparse systems) for the spatial discretization, it will be necessary to turn to a parallel version of the KLE code. This can be done in a relatively easy way: there are several parallel-program packages including parallel versions of the top ODE solvers and evaluation of (38) right-hand side involves matrix products that can be easily paralellizable. Concerning the solution of system (36), back-substitution is essentially a sequential process, then it should be replaced by an iterative parallel linear solver. For a symmetric positive-definite matrix like $\tilde{\boldsymbol{K}}$, the preconditioned conjugate gradient method constitutes the first option, using the triangular factor from an incomplete Cholesky decomposition as preconditioner to accelerate convergence (like before, this incomplete Cholesky factor can be computed once an used repeatedly). Regarding the time integration process, the adaptive ABM-PECE solver works at its best for smooth functions, this situation could change when we try to extend the KLE method to problems with more complex constitutive relations or to the analysis of coupled physical processes where different time scales are likely too appear. If the function is no longer smooth, a recommendable alternative to the ABM-PECE solver is the adaptive Bulirsch–Stoer algorithm with modified midpoint integration and Richardson extrapolation [21]. If different time scales are present, the possibility of stiffness arises and then a Bulirsch–Stoer solver with semi-implicit midpoint integration is recommendable.

As it was mentioned above, the FEM and ABM-PECE techniques were used here for the first implementation of the KLE method. The generality of the KLE method allows further exploration of different techniques for discretization in space and time, which is the author's intention. A particular point to address is the quality of the approximation of the spatial derivatives on the inter-elemental borders and the accuracy of the area-weighing interpolation, specially for nodes that lie at the boundary. In spite that the results shown here exhibit a satisfactory agreement with the experimental measurements, this last issue should be specially taken into account in the choice of space-discretization techniques for future implementations of the KLE method.

Finally, we may emphasize KLE flexibility to manage different trajectories with translational and rotational acceleration and its use of unstructured meshes. This method gives us a useful tool to study the vortex structure of wakes for different body shapes and motions. We are using this tool to explore complex vortex wake patterns in the wake of forced oscillating cylinders at low Reynolds number, focusing on the process of splitting which characterizes the formation of P + S and similar structures. We hope to use the numerical tool developed here to continue with such explorations in the future.

Acknowledgments

F.L.P. is indebted to Hassan Aref for his advice, support and encouragement, and for many valuable discussions. F.L.P. is very grateful to the University of Buenos Aires for granting him a leave in order to complete this work. He also acknowledges the hospitality of the Department of Theoretical and Applied Mechanics at University of Illinois. This work was funded in part by research funds made available by University of Illinois.

References

[1] L. Quartapelle, Numerical Solution of the Incompressible Navier–Stokes Equations, Birkäuser, 1993.

[2] M. Biava, D. Modugno, L. Quartapelle, M. Stopelli, Weak $\psi - \omega$ formulation for unsteady flows in 2D multiply connected domains, J. Comput. Phys. 177 (2002) 209–232.

[3] F. Auteri, L. Quartapelle, L. Vigevano, Accurate $\omega - \psi$ spectral solution of the singular driven cavity problem, J. Comput. Phys. 180 (2002) 597–615.

[4] H.J.H. Clercx, A spectral solver for the Navier–Stokes equations in the velocity–vorticity formulation for flows with two nonperiodic directions, J. Comput. Phys. 137 (1997) 186–211.

[5] C.G. Speziale, On the advantages of the velocity–vorticity formulation of the equations of fluid dynamics, J. Comput. Phys. 73 (1987) 476–480.

[6] H. Fasel, Investigation of the stability of boundary layers by a finite difference model of the Navier–Stokes equations, J. Fluid Mech. 78 (1976) 355–383.

[7] S.C.R. Dennis, D.B. Ingham, R.N. Cook, Finite difference methods for calculating steady incompressible flows in three dimensions, J. Comput. Phys. 33 (1979) 325–339.

[8] T.B. Gatski, C.E. Grosh, M.E. Rose, The numerical solution of the Navier–Stokes equations for 3-dimensional unsteady incompressible flows by compact schemes, J. Comput. Phys. 82 (1989) 298–329.

[9] M. Napolitano, G. Pascazio, A numerical method for the vorticity–velocity Navier–Stokes equations in two and three dimensions, Comput. Fluids 19 (1991) 489–495.

[10] G. Guj, F. Stella, A vorticity–velocity method for the numerical solution of 3D incompressible flows, J. Comput. Phys. 106 (1993) 286–298.

[11] G. Guevremont, W.G. Habashi, P.L. Kotiuga, M.M. Hafez, Finite element solution of the 3D compressible Navier–Stokes equations by a velocity–vorticity method, J. Comput. Phys. 107 (1993) 176–187.

[12] C. Davies, P.W. Carpenter, A novel velocity–vorticity formulation of the Navier–Stokes equations with applications to boundary layer disturbance evolution, J. Comput. Phys. 172 (2001) 119–165.

[13] D.C. Lo, D.L. Young, Arbitrary Lagrangian–Eulerian finite element analysis of free surface flow using a velocity–vorticity formulation, J. Comput. Phys. 195 (2004) 175–201.

[14] C.R. Anderson, Observations on vorticity creation boundary conditions, in: R.E. Caflisch (Ed.), Mathematical Aspects of Vortex Dynamics, SIAM, 1988, pp. 144–159.

[15] A.J. Chorin, Numerical study of slightly viscous flow, J. Fluid Mech. 57 (1973) 785–796.

[16] A.J. Chorin, Vortex sheet approximation of boundary layers, J. Comput. Phys. 27 (1978) 428–442.

[17] L. Quartapelle, F. Valz-Gris, Projections conditions on the vorticity in viscous incompressible flows, Int. J. Numer. Meth. Fluids 1 (1981) 129–144.

[18] L. Quartapelle, Vorticity conditioning in the computation of two-dimensional viscous flows, J. Comput. Phys. 40 (1981) 453–477.

[19] F.L. Ponta, P.M. Jacovkis, Constant-curl Laplacian equation: a new approach for the analysis of flows around bodies, Comput. Fluids 32 (2003) 975–994.

[20] F.L. Ponta, P.M. Jacovkis, A vortex model for Darrieus turbine using finite element techniques, Renewable Energy 24 (2001) 1–18.

[21] W.H. Press, S.A. Teukolsky, W.T. Vetterling, B.P. Flannery, Numerical Recipies in C, second ed., Cambridge University Press, Cambridge, 2002.

[22] K.J. Bathe, Finite Element Procedures, Prentice-Hall, Englewood Cliffs, NJ, 1996.

[23] O.C. Zienkiewicz, R.L. Taylor (Eds.), Finite Element Method, vol. 1, Butterworth-Heinemann, London, 2000.

[24] G.K. Batchelor, An Introduction to Fluid Dynamics, Cambridge University Press, Cambridge, 2000.

[25] M. Van Dyke, An Album of Fluid Motion, Parabolic Press, Stantord, 1982.

[26] S. Taneda, Experimental investigation of the wakes behind cylinders and plates at low Reynolds numbers, J. Phys. Soc. Jpn. 11 (1956) 302–307.

[27] C.H.K. Williamson, Oblique and parallel mode of vortex shedding in the wake of a circular cylinder at low Reynolds numbers, J. Fluid Mech. 206 (1989) 579–627.